

Vicinity Vision Transformer

Weixuan Sun, Zhen Qin, Hui Deng, Jianyuan Wang, Yi Zhang, Kaihao Zhang,
Nick Barnes, Stan Birchfield, Lingpeng Kong, Yiran Zhong

Abstract—Vision transformers have shown great success on numerous computer vision tasks. However, its central component, softmax attention, prohibits vision transformers from scaling up to high-resolution images, due to both the computational complexity and memory footprint being quadratic. Although linear attention was introduced in natural language processing (NLP) tasks to mitigate a similar issue, directly applying existing linear attention to vision transformers may not lead to satisfactory results. We investigate this problem and find that computer vision tasks focus more on local information compared with NLP tasks. Based on this observation, we present a Vicinity Attention that introduces a locality bias to vision transformers with linear complexity. Specifically, for each image patch, we adjust its attention weight based on its 2D Manhattan distance measured by its neighbouring patches. In this case, the neighbouring patches will receive stronger attention than far away patches. Moreover, since our Vicinity Attention requires the token length to be much larger than the feature dimension to show its efficiency advantages, we further propose a new Vicinity Vision Transformer (VVT) structure to reduce the feature dimension without degenerating the accuracy. We perform extensive experiments on the CIFAR100, ImageNet1K, and ADE20K datasets to validate the effectiveness of our method. Our method has a slower growth rate of GFlops than previous transformer-based and convolution-based networks when the input resolution increases. In particular, our approach achieves state-of-the-art image classification accuracy with 50% fewer parameters than previous methods.

Index Terms—Vision Transformer, Image Classification, Linear Transformer, 2D Vicinity, Semantic Segmentation



1 INTRODUCTION

RECENT years have witnessed the success of the transformer structure in natural language processing [1] and computer vision [2]–[4]. However, transformers inherently suffer from quadratic computational complexity and a quadratic memory footprint. As a result, vision transformer methods have to adopt patch-wise image tokenization and pyramid architectures to reduce the sequence length. Despite the temporary relief provided by these methods, the quadratic complexity problem still exists. This limitation prohibits vision transformers from handling high-resolution images or fine-grained image patches.

Linear attention may be a promising direction to solve this issue, which decomposes the self-attention to reduce the computational complexity to linear. Numerous methods have been proposed for attention decomposition, such as approximating the softmax [5]–[7], finding a new similarity metric [8], [9], and so on. However, most of these methods are only verified on NLP tasks, and suffer from a crucial performance drop in computer vision tasks, when compared with conventional softmax attention.

In this paper, we present Vicinity Attention, a new linear attention that is effective in computer vision tasks. Our intuition is based on the fact that convolutional neural networks have dominated computer vision tasks since the rise of deep networks,

and most of them have a locality bias—that is, neighbouring pixels are more likely to be highly related [10]–[15]. Therefore we hypothesize that locality bias is an important property and introduce it into a transformer network. Our re-weighting mechanism is inspired by the recently proposed cosFormer [9], which uses a cosine re-weighting mechanism for 1D NLP tasks. However, directly applying the cosFormer to the vision tasks will lead to unsatisfactory results since the 1D locality enforces stronger connections only on the 1D tokenized neighbouring image patches, is not compatible for 2D distance, *i.e.*, it will assign less weights to vertically connected patches as they are far-away when we tokenized the patches to 1D tokens as shown in Fig 3a. To solve this issue, we propose a 2D Manhattan distance to encourage visual tokens to have a stronger reaction to their neighbors in 2D (Fig 3b-d). Since this mechanism is decomposable, it can be smoothly applied to linear attention.

Comparing with vanilla transformer based methods, our Vicinity Attention can show its efficiency advantages when the sequence length is much larger than the feature dimension. To fulfill this requirement, we propose a new vicinity attention block to reduce the feature dimension without sacrificing performance. It consists a Feature Reduction Attention (RFA) module to reduce the input feature dimension by a half and a Feature Preserving Connection (FRC) to retrieve the original feature distribution and strengthen the representational ability. Following the classic convolutional networks [16], [17], we create a backbone called Vicinity Vision Transformer (VVT) with the vicinity attention block in a pyramid structure. Figure 1a compares our method with current state-of-the-art vision backbones on the ImageNet-1k benchmark. Our method outperforms all the competitors with only half the parameters. We also provide the growth rate of flops with different input resolutions for these methods in Figure 1b. These results demonstrate that our approach can handle larger images than other transformer-based methods as well as convolution-based methods with similar computational costs.

- Weixuan Sun, Jianyuan Wang, Kaihao Zhang, Nick Barnes are with School of Computing, the Australian National University, Canberra, Australia.
- Zhen Qin, Yi Zhang are with SenseTime research, Shanghai, China.
- Hui Deng is with School of Electronics and Information, Northwestern Polytechnical University, Xi'an, China.
- Stan Birchfield is with Nvidia, Redmond, WA, USA.
- Lingpeng Kong is with the University of Hong Kong, Hong Kong, China and Shanghai AI Lab, China.
- Yiran Zhong is with SenseTime Research, Shanghai, China and Shanghai AI Lab, China.
- Weixuan Sun and Zhen Qin are with equal contribution.
- Our code is available at: <https://github.com/OpenNLPLab/Vicinity-Vision-Transformer>.
- Corresponding author: Yiran Zhong (zhongyiran@gmail.com).

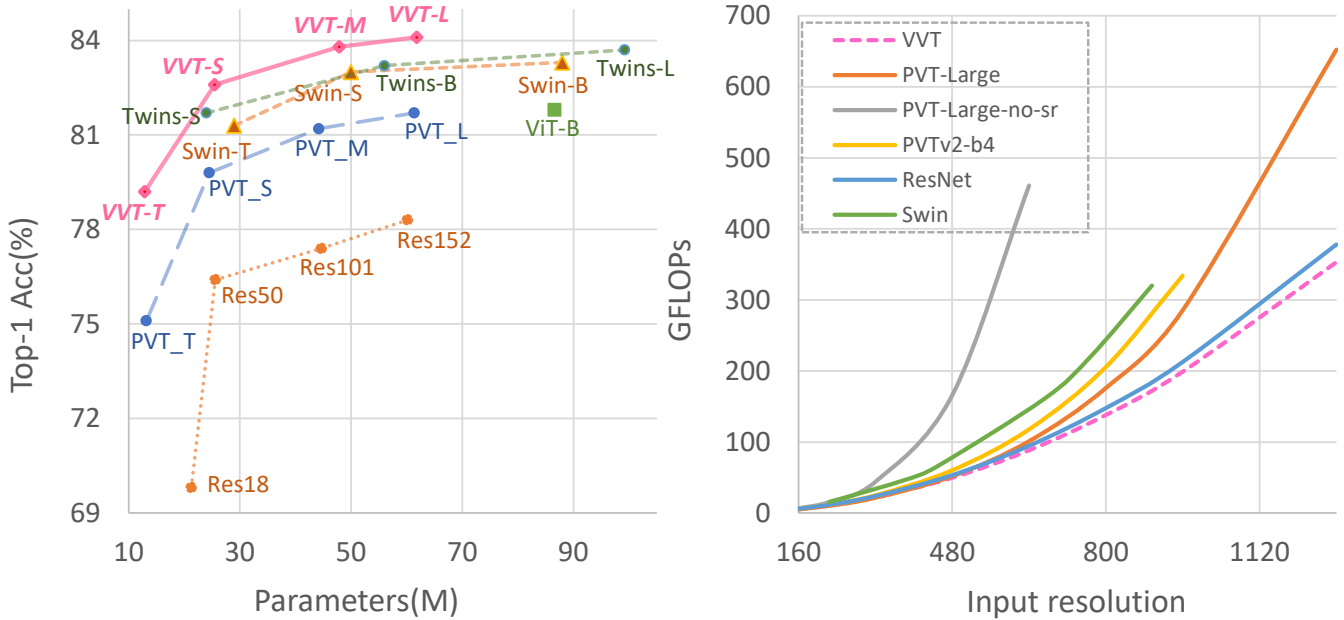


Fig. 1. Top-1 accuracy of our Vicinity Vision Transformer (VVT) with respect to parameters on the ImageNet-1k [18] dataset, and the GFLOPs corresponding to various PVT input image sizes. Our VVT outperforms all competitors with 50% fewer parameters, and it enjoys the lowest GFLOPs growth rate.

Our main contributions are as follows: (1) We propose a new linear vision self-attention module that introduces a 2D Manhattan distance-based locality bias to linear vision transformers. (2) We propose a new multi-head self-attention module called the Vicinity Attention Block, to fulfill the assumption required by Vicinity Attention. It contains a feature reduction attention (FRA) module and a feature preserving connection (FPC) module to control the computational overhead and improve feature extraction ability. (3) We correspondingly build the Vicinity Vision Transformer (VVT), which serves as a general-purpose vision backbone and can be easily applied to vision tasks. Extensive experiments validate the effectiveness of VVT on various computer vision benchmarks.

2 RELATED WORK

2.1 Vision Transformer Backbones

In computer vision tasks, CNN networks have achieved great successes, while recently transformers have gained strong emerging interest. In this section we mainly discuss vision networks using self-attention.

Some works [19]–[21] adopt self-attention mechanisms to replace some or all convolution layers in the CNN networks for image recognition. To further leverage the power of self-attention, [22] proposes a non-local operation and adds it in ResNet [16], the non-local block can capture long-range dependencies and leads to improvements on vision tasks such as video classification, object detection, segmentation, and pose estimation. More recently, pure transformer based vision networks were introduced. ViT [2] splits images into local patches and then projects and flatten patches into embedding sequences, subsequently it employs a pure transformer structure for image classification.

More recently, variations of ViT like CVT [10], Swin [23], PVT [24], Twins [25] and T2T [26] were proposed. CVT [10] introduces Convolutional Token Embedding and Convolutional Projection for Attention to include desirable properties of CNNs into ViT [2] to improve both performance and efficiency. Swin

Transformer [23] introduces non-overlapping windows and applies self-attention in each window, then the window partitions are shifted between adjacent layers. Swin transformer reduces computational complexity and is suitable for different vision tasks. PVT [24] introduces a pure transformer network with a pyramid structure, it further proposes spatial reduction attention which computes self-attention in low dimensions to reduce computation. Twins [25] combines locally-grouped self-attention from Swin [23] and sub-sampled attention from [24], which decreases the computational cost and enhances communications between sub-windows. However, none of the above methods are able to directly process full-length self-attention on high resolution inputs, requiring locally-grouping or sub-sampling. Contrarily, our method can directly calculate self-attention on high-resolution input.

2.2 Efficient Transformers

Various works have been proposed to address the computational complexity problems of transformers in both computer vision and natural language process areas. In addition to vision backbones such as CVT [10], Swin [23], PVT [24], Twins [25] introduced in the previous section, in this section we introduce other more efficient transformer algorithms.

Existing efficient transformer methods can be generally grouped into two categories: pattern-based and kernel-based. Pattern-based methods sparsify the attention matrix with hand-crafted or learnable patterns. [27] reduces the complexity by applying a combination of a strided pattern and a local pattern to the standard attention matrix. Beyond fixed diagonal windows and global windows, Longformer [28] also extends sliding windows with dilation to enlarge the receptive field. Instead of fixed patterns, Reformer [29] and [30] adopt locally sensitive hashing to group tokens into different buckets. On the other hand, kernel-based methods [5]–[7], [9], [31] aim to replace softmax self-attention with approximations or decomposable functions, which

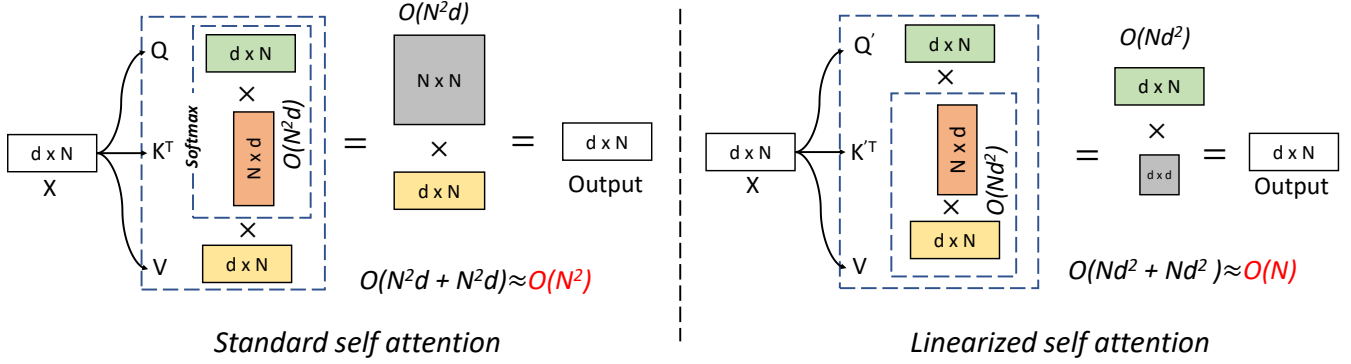


Fig. 2. Illustration of the standard self-attention (left) and linearized self-attention (right). N denotes the patch number of the input image, and d is the feature dimension. With $N \gg d$, the computational complexity of the linearized self-attention grows linearly with respect to the input length, while that of the standard self-attention is quadratic.

change the order of scale dot product calculation and reduce the complexity of self-attention from quadratic to linear.

Two works that are similar to ours are [32] and [33]. [33] applies softmax on Q and K respectively, then changes the dot product order to access a linear complexity. However, it is not validated on a large-scale classification benchmark as a backbone network. SOFT [32] uses a Gaussian kernel function to replace the dot-product similarity in self attention, it assumes that the similarity is symmetrical, which may not hold true in practice. Further, it does not consider the 2D locality mechanism. In this paper, we propose a linear self-attention which facilitates a 2D locality mechanism, and we validate the proposed method on various vision tasks.

3 SELF-ATTENTION, LINEARIZATION, LOCALITY

Self-attention is originally proposed for 1D NLP tasks [1]. To make it suitable for 2D CV tasks, we often convert an image to several patches and then embed them to a sequence $x \in \mathbb{R}^{N \times d}$, where d is the embedding size and $N = \frac{H}{p} \times \frac{W}{p}$ is the patch number, with p , H , W denoting patch size, image height, and image width respectively. Mathematically, a transformer block $\mathcal{T} : \mathbb{R}^{N \times d} \rightarrow \mathbb{R}^{N \times d}$ with input x is defined as:

$$\mathcal{T}(x) = \mathcal{F}(\text{Att}(x) + x), \quad (1)$$

where $\text{Att}(\cdot)$ is the self-attention module and $\mathcal{F}(\cdot)$ is a feed-forward network.

The self-attention module $\text{Att}(\cdot)$ adopts three learnable weights W_Q, W_K, W_V to project x into *query* (Q), *key* (K), and *value* (V). It usually computes an attention matrix A by a similarity function $\mathcal{S}(\cdot)$ over queries and keys. In standard self-attention, $\mathcal{S}(\cdot)$ is softmax normalization. The outputs of the self-attention module is hence $\mathcal{O} = \text{Att}(x) = AV$, where $A \in \mathbb{R}^{N \times N}$ suffers from a quadratic space and time complexity with respect to the patch number N . Therefore, the theoretical computation complexity here is $O(N^2d) = O(\frac{H^2W^2}{p^4}d)$. Consequently the self-attention module becomes sensitive to image size H, W and patch size p , and is the computation bottleneck in vision transformer networks.

Linearization of the self-attention aims to reduce the quadratic theoretical computation complexity to linear. It can be achieved by picking a decomposable similarity function $\mathcal{S}(\cdot)$ to satisfy

$$\mathcal{S}(Q_i, K_j) = \phi(Q_i)\phi(K_j)^\top, \quad (2)$$

where $\phi(\cdot)$ is a kernel function. Given such a kernel, we can write the outputs of the self-attention module as follows:

$$\mathcal{O}_i = \sum_j \frac{\mathcal{S}(Q_i, K_j)}{\sum_j \mathcal{S}(Q_i, K_j)} V_j = \frac{\sum_{j=1}^N (\phi(Q_i)\phi(K_j)^\top) V_j}{\sum_{j=1}^N (\phi(Q_i)\phi(K_j)^\top)} \quad (3)$$

Fig. 2 illustrates the linearization process. Instead of calculating the attention matrix $A \in \mathbb{R}^{N \times N}$, we compute $\phi(K)^\top V \in \mathbb{R}^{d \times d}$ first:

$$[\phi(Q)\phi(K)^\top] V = \phi(Q) [\phi(K)^\top V], \quad (4)$$

such that the $O(N^2d)$ operation is converted to an $O(Nd^2)$ one. Its computational complexity grows linearly with respect to the sequence length N as long as $N \gg d$. A number of linear attention approaches have been proposed for NLP tasks, which use different kernel functions $\phi(x)$ to replace the quadratic softmax, as discussed in the Related Work. However, linear self-attention in vision tasks is not well studied [32], [33] and suffers from a performance drop compared with the standard self-attention module. To address this problem, we propose a linear self-attention that is aware of 2D position.

Locality is a widely used assumption in computer vision [10]–[13], [34]–[38], *i.e.*, neighbouring pixels should have higher possibilities to belong to the same object than distant pixels. Convolution-based networks are inherently coupled with this assumption as they always exploit feature locality [39], [40]. However, this assumption does not hold for standard transformer-based networks due to the self-attention mechanism. Several works show that with the same number of parameters, transformer-based networks cannot match the performance of the CNN counterparts, possibly due to the lack of locality bias [10], [41]. Recent state-of-the-art methods partially introduce locality bias to vision transformers in architecture level, *i.e.*, the Swin transformer [23] uses window self-attention to enforce the locality, PVT [24] adopts pyramid architectures to explore local information, and [10], [13] directly combine convolution with transformers. In this paper, we introduce the locality bias to the self-attention mechanism in linear vision transformers. It can smoothly integrate into existing architecture level locality methods for better performance. In fact, our method achieves better performance than previous state-of-the-art vision transformers in various computer vision benchmarks.

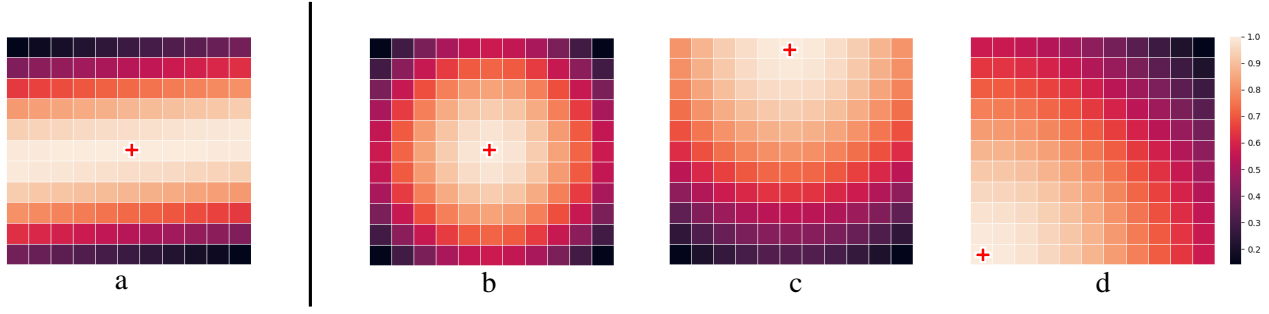


Fig. 3. Visualization of the locality re-weighting patterns. The red cross symbol denotes the query position and the mask denotes the locality weights corresponding to it. We use a lighter color to indicate a larger weight. **(a)** If we directly adopt 1D distance re-weighting [9] in self-attention, the query token will assign lower weights on vertically tokens as they are far away when processed in 1D. **(b), (c), (d)** In our method, Although self-attention is calculated in 1D, our re-weighting mechanism ensures a token is encouraged to have higher relation weights with its neighbours in two dimensions.

4 OUR METHOD

4.1 Vicinity Attention

It has been verified that the softmax normalization is the root of the quadratic complexity of self-attention [32]. In this section, we provide the details of our linear self-attention technique, vicinity attention for vision tasks. The key insight is to replace the standard softmax operation by another similarity function, which (1) can be decomposed to simple kernel functions and (2) introduces a locality constraint that is beneficial in visual understanding. Inspired by [9], we adopt $\text{ReLU}(\cdot)$ as the kernel function, and conduct a row-wise normalization to replace softmax. Our self-attention then can be reformulated as:

$$\begin{aligned} \mathcal{O}_i &= \frac{\sum_{j=1}^N [\text{ReLU}(Q_i) \text{ReLU}(K_j)^\top] V_j}{\sum_{j=1}^N [\text{ReLU}(Q_i) \text{ReLU}(K_j)^\top]} \\ &= \frac{\text{ReLU}(Q_i) \sum_{j=1}^N [\text{ReLU}(K_j)^\top V_j]}{\text{ReLU}(Q_i) \sum_{j=1}^N \text{ReLU}(K_j)^\top} \end{aligned} \quad (5)$$

where we can reorder the calculation so the complexity is reduced to linear with respect to the sequence length N . This ReLU-based normalization method retains two important properties of standard self-attention: (1) it is always positive, avoiding aggregating negatively-correlated information. (2) all the elements lie between $[0, 1]$.

Enforcing 2D Locality Bias The locality bias has been discussed in language tasks [9], [42], [43] with 1D sequence distance encoding. In vision transformers, the embedding sequence is flattened from a 2D mask, hence it is essential to consider token positions in 2D before flattening. To enforce the locality bias in linear transformers, we need a kernel function that can 1) put more weight on neighbouring patches and 2) can be decomposed with Eq. (2).

Given two tokens q_i, k_j from Q and K respectively, the positions of these two tokens on the 2D feature maps before flattening are:

$$i = u_i m + r_i, \quad j = u_j m + r_j, \quad 0 \leq r_i, r_j < m \quad (6)$$

where m is width of the feature map, u denotes the row index, and r denotes the column index. Following Eq. (2), we can define a re-weighted attention with a distance function \mathcal{D} to enforce the locality bias between neighbouring tokens as:

$$\mathcal{S}(Q_i, K_j) = \phi(Q_i) \mathcal{G}(\mathcal{D}(i, j)) \phi(K_j)^\top \quad (7)$$

where \mathcal{G} generates the weight according to the distance. A naive choice might be directly using the Euclidean distance $\sqrt{(r_j - r_i)^2 + (u_j - u_i)^2}$. Since this term cannot be decomposed into two terms relating to i and j separately, it cannot be applied to the linear transformers.

Instead, we propose to use the 2D Manhattan distance [44] as the distance function, which can be easily decoupled into the distance in two directions. However, in direct Manhattan distance decoupling is still hindered:

$$\mathcal{S}(Q_i, K_j) = \phi(Q_i) \mathcal{G}(|r_j - r_i| + |u_j - u_i|) \phi(K_j)^\top$$

as the absolute operation cannot be decomposed.

To fulfill the aforementioned requirements, we propose a 2D cos-based re-weighting mechanism for our self-attention module. First, given the feature map with size m by n , following Eq. (6) we redefine the 2D positions as:

$$a_i = \frac{\pi u_i}{2n}, \quad a_j = \frac{\pi u_j}{2n}, \quad b_i = \frac{\pi r_i}{2m}, \quad b_j = \frac{\pi r_i}{2m} \quad (8)$$

Then, using the Manhattan distance, the self-attention calculation can be decomposed into four terms:

$$\begin{aligned} \mathcal{S}(Q_i, K_j) &= \phi(Q_i) (\cos(a_i - a_j) + \cos(b_i - b_j)) \phi(K_j)^\top \\ &= \phi(Q_i) (\cos(a_i) \cos(a_j)) \phi(K_j)^\top + \\ &\quad \phi(Q_i) (\sin(a_i) \sin(a_j)) \phi(K_j)^\top + \\ &\quad \phi(Q_i) (\cos(b_i) \cos(b_j)) \phi(K_j)^\top + \\ &\quad \phi(Q_i) (\sin(b_i) \sin(b_j)) \phi(K_j)^\top \\ &= \phi^{\cos a_i}(Q_i) \phi^{\cos a_j}(K_j)^\top + \\ &\quad \phi^{\sin a_i}(Q_i) \phi^{\sin a_j}(K_j)^\top + \\ &\quad \phi^{\cos b_i}(Q_i) \phi^{\cos b_j}(K_j)^\top + \\ &\quad \phi^{\sin b_i}(Q_i) \phi^{\sin b_j}(K_j)^\top \end{aligned} \quad (9)$$

where $\phi^{\cos y}(x) \triangleq \cos(y) \phi(x)$, $\phi^{\sin y}(x) \triangleq \sin(y) \phi(x)$.

The detailed derivation is included in the supplementary materials. Here the queries and keys are related to their own positions i and j , and hence we can fulfill the Eq. (4) to reorder the dot product in self-attention. Our method provides three appealing properties: (1) *Linear complexity*: cosine can be decomposed, thus KV is calculated first to ensure linear complexity. (2) *Locality bias*: if two tokens are close to each other in 2D feature maps, they are encouraged to have stronger relationships, as shown in

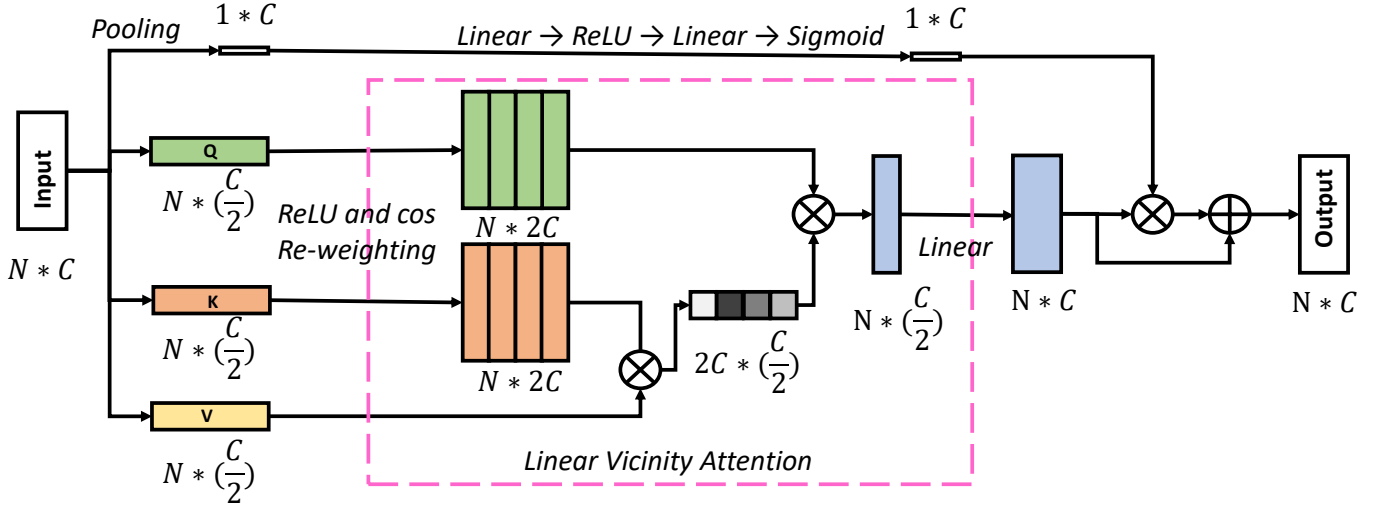


Fig. 4. Illustration of the Vicinity Attention Block. The input feature dimension is down-sampled to reduce the computational cost, while the original feature distribution is retained by the Feature Preserving Connection.

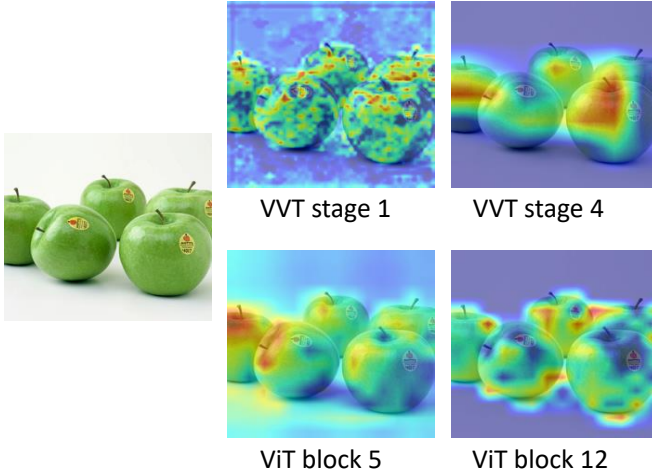


Fig. 5. Grad_CAM of the proposed network and ViT [2]. Our network can generate high-resolution feature maps in early stages, which contain more fine-grained local object features.

Fig. 3. (3) *Global context*: it retains a global receptive field as in the standard self-attention.

4.2 Vicinity Attention Block

The theoretical computational complexity of Vicinity Attention is $O(N(4d)^2)$. To achieve a linear computational complexity, the sequence length N should be much larger than the feature dimension d . To ensure the computational cost is close to linear, we redesign the structure of multi-head self-attention (MSA) module to reduce the feature dimension without hindering the performance.

We present a schematic illustration of our Vicinity Attention Block in Fig. 4. It receives an input $X \in \mathbb{R}^{N \times d}$, which is projected into $Q \in \mathbb{R}^{N \times \frac{d}{2}}$, $K \in \mathbb{R}^{N \times \frac{d}{2}}$, $V \in \mathbb{R}^{N \times \frac{d}{2}}$ with a reduced feature dimension. We call it Feature Reduction Attention (FRA). Then, following our locality decomposition in Eq. (9), we obtain $Q' \in \mathbb{R}^{N \times 2d}$, $K' \in \mathbb{R}^{N \times 2d}$ which is used to calculate linear self-attention. After that, since our self-attention is calculated in lower

dimensions, we add a skip connection called Feature Preserving Connection (FRC) which has negligible computational overhead ($O(2d^2)$). We also adopt an average pooling operation and two linear layers to retain the original feature distribution and strengthen the representational ability. Given the feature dimension is reduced by 2, our current computational complexity is $O(N(2d)^2 + 2d^2)$.

In Figure 5, we show some qualitative examples of Grad-CAM [45] obtained from the proposed VVT and ViT [2]. Our approach is able to produce fine-grained features whereas the ViT [2] can only capture low-resolution features.

4.3 The Vicinity Vision Transformer

To validate the effectiveness of our idea, we propose a general-purpose vision backbone called Vicinity Vision Transformer (VVT), as shown in Fig. 6. VVT adopts a progressive shrinking pyramid structure and has four stages that generate feature maps at different scales. Each stage contains a patch embedding layer and multiple Vicinity Transformer Blocks. In detail, we use a patch size of 4×4 in the first stage. Given the input image of size $H \times W \times 3$, we first divide it into $\frac{H}{4} \times \frac{W}{4}$ patches. Then we feed the patches into a patch embedding module to obtain a flattened embedding sequence with size of $\frac{HW}{4^2} \times C_1$. Here we adopt the patch embedding module proposed by [46] to project the patches into the target feature embedding. The embedding sequence is subsequently fed into several successive transformer blocks with L_1 layers.

Compared with the standard transformer block, we only replace the multi-head self-attention (MSA) module with our proposed linear Vicinity Attention Block, while other parts are kept the same. In the second stage, the feature sequence from the first stage is reshaped back to $\frac{H}{4} \times \frac{W}{4} \times C_1$ and fed into the patch embedding module again. It is projected and down-sampled to a embedding sequence of size $\frac{HW}{8^2} \times C_2$, and then processed by the transformer blocks of the second stage. We follow the same approach to obtain multi-scale output feature maps of the third and fourth stage with output sizes of $\frac{H}{16} \times \frac{W}{16}$ and $\frac{H}{32} \times \frac{W}{32}$, respectively. Hierarchical feature maps can be easily leveraged to many downstream tasks such as image classification, semantic segmentation and object detection. Similar to other backbone

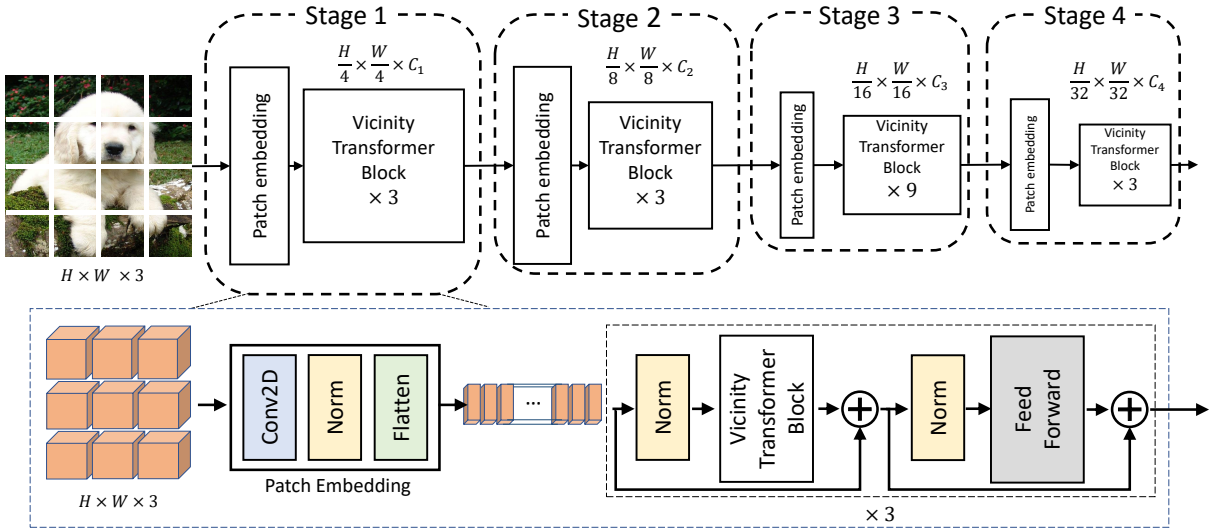


Fig. 6. Overall architecture of our VVT. VVT adopts a pyramid structure and is divided into four stages. The illustrated sample is VVT-Small. The output resolution progressively shrinks to generate multi-scale feature maps.

TABLE 1

Detailed specifications of our VVT variants. We show four variants of our VVT structure. C: Feature dimension, P: Patch size, R: Feature reduction, H: Head number, E: Expansion ratio of the feed-forward layer. Following Swin Transformer [23], the layers amount of the four stages follow the ratios of 1 : 1 : 3 : 1 or 1 : 1 : 9 : 1.

	Output Size	Layer Name	Tiny	Small	Medium	Large
Stage 1	$\frac{H}{4} \times \frac{W}{4}$	Patch Embedding	C = 96, P = 4			
		Transformer Encoder	$\begin{matrix} R = 2 \\ H = 1 \\ E = 8 \end{matrix} \times 2$	$\begin{matrix} R = 2 \\ H = 1 \\ E = 8 \end{matrix} \times 3$	$\begin{matrix} R = 2 \\ H = 1 \\ E = 8 \end{matrix} \times 3$	$\begin{matrix} R = 2 \\ H = 1 \\ E = 4 \end{matrix} \times 4$
Stage 2	$\frac{H}{8} \times \frac{W}{8}$	Patch Embedding	C = 160, P = 2			
		Transformer Encoder	$\begin{matrix} R = 2 \\ H = 2 \\ E = 8 \end{matrix} \times 2$	$\begin{matrix} R = 2 \\ H = 2 \\ E = 8 \end{matrix} \times 3$	$\begin{matrix} R = 2 \\ H = 2 \\ E = 8 \end{matrix} \times 3$	$\begin{matrix} R = 2 \\ H = 2 \\ E = 4 \end{matrix} \times 4$
Stage 3	$\frac{H}{16} \times \frac{W}{16}$	Patch Embedding	C = 320, P = 2			
		Transformer Encoder	$\begin{matrix} R = 2 \\ H = 5 \\ E = 4 \end{matrix} \times 2$	$\begin{matrix} R = 2 \\ H = 5 \\ E = 4 \end{matrix} \times 9$	$\begin{matrix} R = 2 \\ H = 5 \\ E = 4 \end{matrix} \times 27$	$\begin{matrix} R = 2 \\ H = 5 \\ E = 4 \end{matrix} \times 36$
Stage 4	$\frac{H}{32} \times \frac{W}{32}$	Patch Embedding	C = 512, P = 2			
		Transformer Encoder	$\begin{matrix} R = 2 \\ H = 8 \\ E = 4 \end{matrix} \times 2$	$\begin{matrix} R = 2 \\ H = 8 \\ E = 4 \end{matrix} \times 3$	$\begin{matrix} R = 2 \\ H = 8 \\ E = 4 \end{matrix} \times 3$	$\begin{matrix} R = 2 \\ H = 8 \\ E = 4 \end{matrix} \times 4$

methods, we introduce different architecture variants like VVT-Tiny or VVT-Large, whose details are shown in Table 1.

5 EXPERIMENTS

To verify the effectiveness of our method, we conduct extensive experiments on the CIFAR100 [47] and ImageNet1K [39] datasets for image classification, and on the ADE20K [48] dataset for semantic segmentation. Specifically, we first make a comparison with existing state-of-the-art methods, and then give an ablation study over the design of VVT.

5.1 Image Classification

The image classification experiments are conducted on the ImageNet1K [39] dataset, which contains 1.28 million training images and 50 thousand validation images from 1,000 categories. We follow the training hyper-parameters of PVT [24] for a fair comparison. In detail, the model is trained using an AdamW [53] optimizer with a weight decay of 0.05 and a momentum of 0.9.

We use an initial learning rate of 5×10^{-4} and decrease it by a cosine schedule [54], with 5 epochs for warming up. We also adopt the same data augmentation strategy as in [24], including random cropping, random horizontal flipping, etc. All the models are trained on the training set for 300 epochs with a crop size of 224×224 . We use the top-1 accuracy as the evaluation metric.

The quantitative results are shown in Table 2, which covers the popular transformer-based and CNN-based classification networks. We compare the VVT variants respectively with the networks using similar parameters, split by solid lines. For example, VVT-L performs better than PVTv2-B5 [24] but only uses around 70% parameters of the latter. In particular, our medium-size variant VVT-M surpasses the large models Twins-SVT-L [25] and Swin-B [23] with substantially fewer parameters (51.7% and 45.5% respectively). Moreover, compared to the state-of-the-art CNN-based networks such as RegNet [55] and ResNeXt [52], VVT shows stronger performance while using a similar number of parameters.

It is worth noting that VVT directly computes self-attention

TABLE 2

Comparison of different backbones on ImageNet1k [39]. All models are trained and tested on 224×224 resolution. GFLOPs is also calculated under the input scale of 224×224 . MS out represents multi-scale output.

Method	Style	Resolution	MS out	Param	GFLOPs	Top-1 Acc(%)
ResNet18 [16]	ConvNets	224^2	✓	11.7	1.8	69.8
DeiT-Tiny/16 [49]	Transformers	224^2	✗	5.7	1.3	72.2
PVTv2-B1 [46]	Transformers	224^2	✓	13.1	2.1	78.7
VVT-T(ours)	Transformers	224^2	✓	12.9	3.0	79.2
ResNet50 [16]	ConvNets	224^2	✓	25.6	4.1	76.1
PVT-Small [24]	Transformers	224^2	✓	24.5	3.8	79.8
RegNetY-4G [50]	ConvNets	224^2	✓	21.0	4.0	80.0
TNT-S [11]	Transformers	224^2	✗	23.8	5.2	81.3
Swin-T [23]	Transformers	224^2	✓	29.0	4.5	81.6
CvT-13 [10]	Hybrid	224^2	✓	20.0	4.5	81.6
Twins-SVT-S [25]	Hybrid	224^2	✓	24.0	2.8	81.7
XCiT-S12 [51]	Linear Transformers	224^2	✗	26.0	4.8	82.0
PVTv2-B2-Li [46]	Transformers	224^2	✓	22.6	3.9	82.1
SOFT [32]	Linear Transformers	224^2	✓	24.0	3.3	82.2
VVT-S(ours)	Linear Transformers	224^2	✓	25.5	5.6	82.6
ResNet101 [16]	ConvNets	224^2	✓	44.7	7.9	77.4
ViT-Small16 [2]	Transformers	224^2	✗	48.8	9.9	80.8
PVT-Medium [24]	Transformers	224^2	✓	44.2	6.7	81.2
RegNetY-8G [50]	ConvNets	224^2	✓	39.0	8.0	81.7
CvT-21 [10]	Hybrid	224^2	✓	32.0	7.1	82.5
XCiT-S24 [51]	Linear Transformers	224^2	✗	48.0	9.1	82.6
SOFT [32]	Linear Transformers	224^2	✓	45.0	7.2	82.9
Swin-S [23]	Transformers	224^2	✓	50.0	8.7	83.0
Twins-SVT-B [25]	Hybrid	224^2	✓	56.0	8.3	83.2
PVTv2-B3 [46]	Transformers	224^2	✓	45.2	6.9	83.2
PVTv2-B4 [46]	Transformers	224^2	✓	62.6	10.1	83.6
VVT-M(ours)	Linear Transformers	224^2	✓	47.9	9.4	83.8
ResNet152 [16]	ConvNets	224^2	✓	60.2	11.6	78.3
PVT-Large [24]	Transformers	224^2	✓	61.4	9.8	81.7
ViT-Base16 [2]	Transformers	224^2	✗	86.6	16.0	81.8
T2T-ViT-24 [26]	Transformers	224^2	✓	63.9	13.2	82.2
XCiT-M24 [51]	Linear Transformers	224^2	✗	84.0	16.2	82.7
ResNeXt101-64x4d [52]	ConvNets	224^2	✓	84.0	16.0	82.9
TNT-B [11]	Transformers	224^2	✗	65.6	14.1	82.9
RegNetY-16G [50]	ConvNets	224^2	✓	84.0	16.0	82.9
SOFT [32]	Linear Transformers	224^2	✓	64.0	11.0	83.1
Swin-B [23]	Transformers	224^2	✓	88.0	15.4	83.3
Twins-SVT-L [25]	Hybrid	224^2	✓	99.2	14.8	83.7
PVTv2-B5 [46]	Transformers	224^2	✓	82.0	11.8	83.8
VVT-L(ours)	Linear Transformers	224^2	✓	61.8	10.8	84.1

on the high-resolution feature maps, while the competitors such as PVT [24], Swin Transformer [23], Twins [25] and SOFT [32] rely on the sub-sampling or window self-attention to reduce computational cost. The GFLOPs of VVT could be further reduced if similar subsampling or windowing was used.

5.2 Semantic Segmentation

We utilize the challenging ADE20K [48] dataset to evaluate our idea in semantic segmentation. It has 150 semantic classes, with 20, 210, 2,000 and 3,352 images for training, validation and testing. With the VVT models (pre-trained on ImageNet1K) as

the backbone, we provide the results using two segmentation methods in Table 3. Specifically, we pick Semantic FPN [56] and UperNet [57] as the semantic segmentation architecture, respectively following the settings of PVT [24] and Swin Transformer [23]. The quantitative results show that our method is consistently superior to the competing CNN-based methods. For example, using Semantic FPN, VVT-S outperforms ResNet50 [16] by 8.9%, and VVT-L is 7.7% better than ResNeXt101-32x4d [52], using mIoU as the metric. VVT also shows a more favourable segmentation result than the transformer-based competitors such as the Swin Transformer. A similar phenomenon is observed if

TABLE 3

Semantic segmentation results on ADE20K [48] validation set. Competing results come from PVTv2 [46] and Twins [25]. All backbone networks are pre-trained on ImageNet1k [39].

Method	Semantic FPN(PVT [24] setting)			Upernet(Swin [23] setting)		
	Params	GFLOPs	mIoU(%)	Params	GFLOPs	mIoU(%)
ResNet50 [16]	28.5	45.6	36.7	-	-	-
PVT-Small [24]	28.2	44.5	39.8	-	-	-
Swin-T [23]	31.9	46.0	41.5	59.9	237	44.5
Twins-SVT-S [25]	28.3	37.0	43.2	54.4	228	46.2
PVTv2-b2 [46]	29.1	45.8	45.2	-	-	-
VVT-S(ours)	29.2	50.9	45.6	55.5	240	46.8
ResNet101 [16]	47.5	65.1	38.8	-	-	-
ResNeXt101-32x4d [52]	47.1	64.7	39.7	-	-	-
PVT-Medium [24]	51.6	61.0	41.6	-	-	-
SWIN-S [23]	53.2	70.0	45.2	81.3	261	47.6
Twins-SVT-B [25]	60.4	67.0	45.3	88.5	261	47.7
PVTv2-b3 [46]	49.0	62.4	47.3	-	-	-
VVT-M(ours)	51.7	70.8	47.4	77.9	260	48.1
ResNeXt101-64x4d [52]	86.4	103.9	40.2	-	-	-
PVT-Large [24]	65.1	79.6	42.1	-	-	-
SWIN-B [23]	91.2	107.0	46.0	121	299	48.1
Twins-SVT-L [25]	103.7	102.0	46.7	133	297	48.8
PVTv2-b4 [46]	66.3	81.3	47.9	-	-	-
VVT-L(ours)	65.5	78.1	47.9	91.9	267	48.8

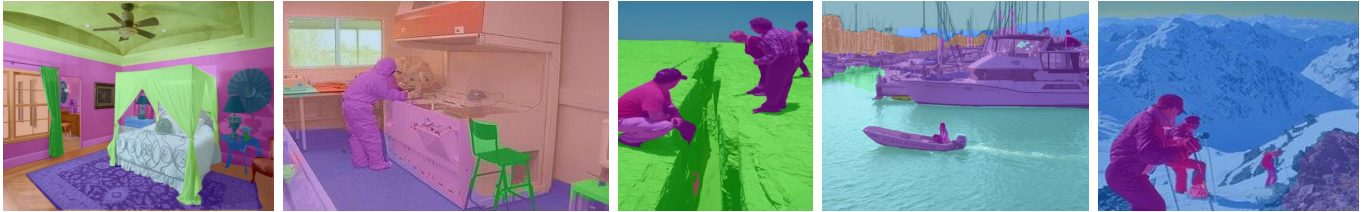


Fig. 7. Qualitative results of semantic segmentation on ADE20K [48]. The results are generated by VVT-L based Semantic FPN [56].

taking UperNet [57] as the segmentation method. These results validate that the extracted features of VVT are also valuable for semantic segmentation, which benefits from the locality mechanism together with the global attention.

5.3 Ablation Study

Computational Overhead. We plot the GFLOPs growth rates with respect to the input image size on the right of Fig. 1. The GFLOPs growth rate of VVT (purple) is substantially lower than other transformer-based methods, and even slightly lower than ResNet [16]. Note that PVT [24] down-samples the sequence length to reduce the computational complexity, whereas we directly compute self-attention without any spatial reduction. If PVT computes self-attention on the full-length inputs (labeled as PVT_no_SR, grey in Fig. 1), its GFLOP growth rate becomes notably larger and will exhaust the GPU memory (32G) once the image size exceeds 640×640 . This ablation study validates that VVT successfully mitigates the computational issue in the vision transformers.

Effect of Locality Constraint. The *Vicinity* locality mechanism is introduced in the self-attention module of VVT. We show its effectiveness on the CIFAR-100 [47] and the ImageNet1K [39] datasets in Table 4. Experiments are performed on the VVT-Tiny structure.

TABLE 4

Analysis of locality constraint on Cifar100 [47] and ImageNet1K [39]. The VVT-softmax represents the variant that replaces all Vicinity Attention with the standard softmax attention.

Datasets	Method	Top-1 Acc(%)
Cifar100	PVT [24]	81.67
	VVT-softmax	82.68
	VVT w/o locality	82.13
	VVT 1D locality	76.78
	VVT 2D locality	82.92
ImageNet1K	VVT w/o locality	78.0
	VVT 2D locality	79.2

We compare the VVT with the one without locality (denoted as VVT w/o locality) and the one with 1D locality (denoted as VVT 1D locality). We add the state-of-the-art vision transformer PVT [24] as our reference. For the sake of completeness, we also provide a VVT variant that replaces all Vicinity Attention with the standard softmax attention, and denote it as the VVT-softmax. As shown in the table, our VVT achieves the best performance among all the others, even better than the one with standard softmax attention while it also has only linear computation complexity. By comparing the VVT w/o locality and VVT 1D locality, we can find

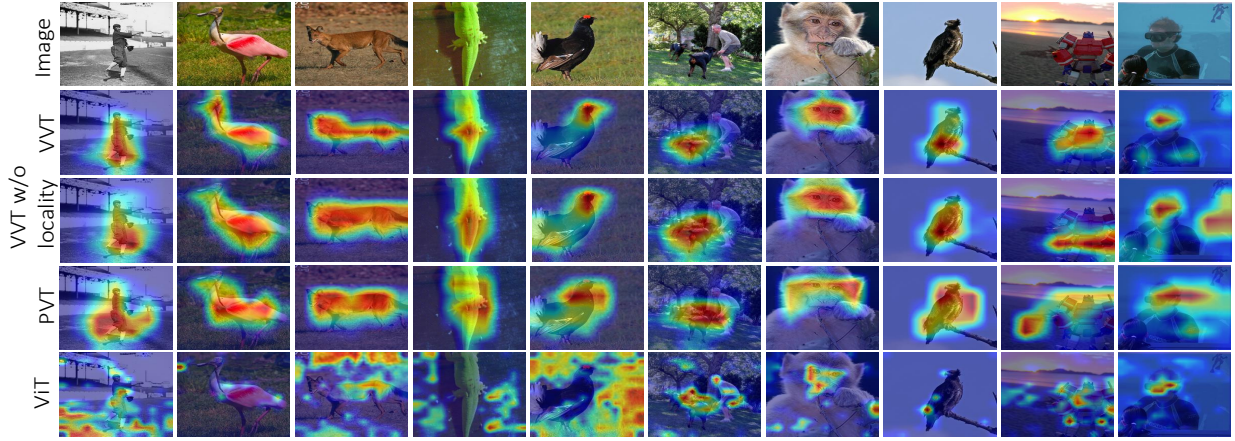


Fig. 8. We compare the class-wise attention maps of the VVT against the VVT w/o locality, the PVT [24] and the ViT [2]. The attention maps are obtained using Grad_CAM [45]. By enforcing the locality bias, the activation areas are more concentrated and correctly locate on the object.

TABLE 5
Ablation of different attention choices. We fix the architecture to VVT-T and test different attention modules on Cifar100.

Architecture	Attention	Param	Top-1 Acc(%)
VVT-T	Efficient attention [33]	12.4	81.63
VVT-T	Performer [7]	12.4	79.86
VVT-T	Linformer [31]	13.1	80.95
VVT-T	PVTv2 [46]	15.2	82.16
VVT-T	Vanilla [1]	12.4	82.68
VVT-T	Ours	12.4	82.92

that if we wrongly enforce the locality bias, the performance will drop critically. To further demonstrate its effectiveness on large-scale data, we also conduct the ablation on the ImageNet1K [18], where our VVT outperforms the VVT w/o locality by 1.2%.

Furthermore, we show the qualitative examples of Grad-CAM [45] from VVT and the competitors in Fig. 8. As shown, the locality mechanism encourages the tokens to assign higher attention to 2D neighbours, and hence the class-wise activations are more concentrated and accurately located on the target object regions of Grad-CAM. These results validate that the introduction of the 2D locality mechanism helps the VVT models generate more reliable object features, which tend to be beneficial in image classification and downstream tasks.

Analysis of Vicinity Attention. In order to demonstrate the effectiveness of our proposed Vicinity attention module solely. We adopt same network structure and replace Vicinity attention with other efficient attention modules including vanilla attention [1], Performer [7], Linformer [31], PVTv2 [46] and [33]. Results on Cifar100 are reported in Table 5. As shown, under the same network architecture setting, our Vicinity attention outperforms both the vanilla attention and all the alternative efficient ones.

Analysis of Feature Reduction. In the Vicinity Attention Block, we reduce the feature dimension to fulfill the assumption of $N \gg d$, which forces the computational complexity to approach linear. In Fig. 9, we ablate the computational cost under different feature reduction (FR) ratios. We can observe an obvious GFLOPs decrease when increasing the FR ratio from 1 to 2 (reducing the feature dimension by half). However, when the FR ratio further increases, the reduction tends to saturate. This is because the computational cost of the self-attention module is already

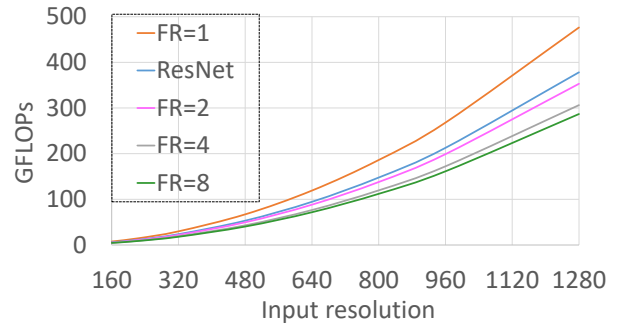


Fig. 9. GFLOPs of VVT using different feature reduction rates. When FR ratio is increased larger than 4, the growth ratio tends to be saturated.

TABLE 6
Results of VVT using different feature reduction ratio(FR). We empirically find that the FR = 2 leads to the best performance.

Method	Feature Reduction ratio	Top-1 Acc(%)
PVT [24]	-	81.67
VVT	FR=1	82.89
VVT	FR=2	82.92
VVT	FR=4	82.00
VVT	FR=8	80.60

significantly reduced and the other model parts dominate the computational overhead. Additionally, we ablate the performances under different FR ratios on the Cifar100 dataset, as shown in Table 6. As shown, when the FR ratio is small, the model retains a similar performance (e.g., 82.89% vs. 82.92%), indicating that the feature representation ability is not affected. When the FR ratio increases to a number like 8, a clear performance drop is observed. As a trade-off, we set the FR ratio as 2 for our formal model settings.

Feature Preserving Connection. In the Vicinity Attention Block, feature preserving connections are added to compensate reduced feature dimensions. Ablation of feature preserving connection is reported in Table 7. The results indicate that feature preserving connection effectively retains original feature distribution, and improves feature extraction ability of Vicinity attention module

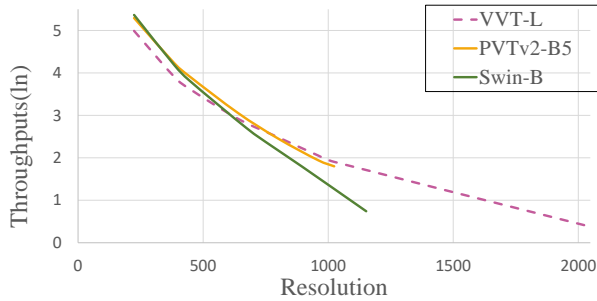


Fig. 10. Throughputs-resolution curve. We take \log of throughputs for better readability.

even feature dimension is reduced.

TABLE 7
Results of VVT-tiny with and without feature preserving connection(FPC) on ImageNet1k.

Method	Feature Preserving Connection	Top-1 Acc(%)
VVT	✗	77.9
VVT	✓	79.2

Image Classification with Different Input Size Table 8 lists the performances of VVT with a higher input resolution i.e., 384. Obviously, larger input resolution leads to better top-1 accuracy but requires larger computation. Compared to Swin [23], VVT achieves better results with similar or lower computational overhead.

Image Classification Throughputs Fig.10 illustrates actual image throughputs of the proposed VVT compared to PVTv2 [46] and Swin transformer [23], we run the test on one local 2080 Ti GPU with 10 Gb memory. Since the theoretical computational complexity of Vicinity attention is $O(N(2d)^2 + 2d^2)$, in low resolution regime where sequence length N does not dominate the complexity, VVT shows relatively slow speed compared to PVTv2 [46] and Swin [23]. However, when input resolution is gradually increased, the VVT starts demonstrating better inference speed, while competing methods exhaust GPU memory in the high resolution regime.

6 CONCLUSION

We have introduced Vicinity Vision Transformer (VVT), a general-purpose vision backbone that produces hierarchical feature representations through a pyramid structure. At its core, VVT uses a novel Vicinity Attention Block, which introduces a 2D locality mechanism into the self-attention module. We validate that this locality mechanism improves results and helps generate better class activations. Further, because Vicinity Attention has linear complexity, it facilitates processing feature maps or input images with higher resolutions. The proposed VVT has been validated with strong performance on both image classification and semantic segmentation. Future work will be aimed at using neural architecture search to further improve upon architectures specifically designed for linear vision transformers.

REFERENCES

[1] A. Vaswani, N. Shazeer, N. Parmar, J. Uszkoreit, L. Jones, A. N. Gomez, L. Kaiser, and I. Polosukhin, "Attention is all you need," *Advances in neural information processing systems*, vol. 30, 2017.

TABLE 8
Classification results on ImageNet1k under the input scale 384 × 384.

Method	Param	GFLOPs	Top-1 Acc(%)
VVT-T	12.9	8.8	80.3
Swin-T [23]	29.0	14.0	82.2
VVT-S	25.5	16.5	83.4
Swin-B [23]	88.0	47.0	84.5
VVT-L	61.8	31.8	84.7

[2] A. Dosovitskiy, L. Beyer, A. Kolesnikov, D. Weissenborn, X. Zhai, T. Unterthiner, M. Dehghani, M. Minderer, G. Heigold, S. Gelly, *et al.*, "An image is worth 16x16 words: Transformers for image recognition at scale," *arXiv preprint arXiv:2010.11929*, 2020.

[3] X. Cheng, H. Xiong, D.-P. Fan, Y. Zhong, M. Harandi, T. Drummond, and Z. Ge, "Implicit motion handling for video camouflaged object detection," in *Proceedings of the IEEE/CVF Conference on Computer Vision and Pattern Recognition*, pp. 13864–13873, 2022.

[4] W. Sun, J. Zhang, Z. Liu, Y. Zhong, and N. Barnes, "GETAM: gradient-weighted element-wise transformer attention map for weakly-supervised semantic segmentation," *CoRR*, vol. abs/2112.02841, 2021.

[5] Y. Xiong, Z. Zeng, R. Chakraborty, M. Tan, G. Fung, Y. Li, and V. Singh, "Nystromformer: A nystrom-based algorithm for approximating self-attention," in *Proceedings of the... AAAI Conference on Artificial Intelligence*. AAAI Conference on Artificial Intelligence, vol. 35, p. 14138, NIH Public Access, 2021.

[6] H. Peng, N. Pappas, D. Yogatama, R. Schwartz, N. A. Smith, and L. Kong, "Random feature attention," *arXiv preprint arXiv:2103.02143*, 2021.

[7] K. Choromanski, V. Likhoshesterov, D. Dohan, X. Song, A. Gane, T. Sarlos, P. Hawkins, J. Davis, A. Mohiuddin, L. Kaiser, *et al.*, "Rethinking attention with performers," *arXiv preprint arXiv:2009.14794*, 2020.

[8] A. Katharopoulos, A. Vyas, N. Pappas, and F. Fleuret, "Transformers are rnns: Fast autoregressive transformers with linear attention," in *International Conference on Machine Learning*, pp. 5156–5165, PMLR, 2020.

[9] Q. Zhen, W. Sun, H. Deng, D. Li, Y. Wei, B. Lv, J. Yan, L. Kong, and Y. Zhong, "cosformer: Rethinking softmax in attention," in *International Conference on Learning Representations*, 2022.

[10] H. Wu, B. Xiao, N. Codella, M. Liu, X. Dai, L. Yuan, and L. Zhang, "Cvt: Introducing convolutions to vision transformers," in *Proceedings of the IEEE/CVF International Conference on Computer Vision*, pp. 22–31, 2021.

[11] K. Han, A. Xiao, E. Wu, J. Guo, C. Xu, and Y. Wang, "Transformer in transformer," *Advances in Neural Information Processing Systems*, vol. 34, 2021.

[12] L. Yuan, Y. Chen, T. Wang, W. Yu, Y. Shi, Z.-H. Jiang, F. E. Tay, J. Feng, and S. Yan, "Tokens-to-token vit: Training vision transformers from scratch on imagenet," in *Proceedings of the IEEE/CVF International Conference on Computer Vision*, pp. 558–567, 2021.

[13] Z. Dai, H. Liu, Q. Le, and M. Tan, "Coatnet: Marrying convolution and attention for all data sizes," *Advances in Neural Information Processing Systems*, vol. 34, 2021.

[14] Y. Zhong, Y. Dai, and H. Li, "Self-supervised learning for stereo matching with self-improving ability," *arXiv preprint arXiv:1709.00930*, 2017.

[15] Y. Zhong, Y. Dai, and H. Li, "Stereo computation for a single mixture image," in *Proceedings of the European Conference on Computer Vision (ECCV)*, September 2018.

[16] K. He, X. Zhang, S. Ren, and J. Sun, "Deep residual learning for image recognition," in *Proceedings of the IEEE Conference on Computer Vision and Pattern Recognition*, pp. 770–778, 2016.

[17] T.-Y. Lin, P. Dollár, R. Girshick, K. He, B. Hariharan, and S. Belongie, "Feature pyramid networks for object detection," in *Proceedings of the IEEE conference on computer vision and pattern recognition*, pp. 2117–2125, 2017.

[18] A. Krizhevsky, I. Sutskever, and G. E. Hinton, "Imagenet classification with deep convolutional neural networks," *Advances in neural information processing systems*, vol. 25, 2012.

[19] H. Hu, Z. Zhang, Z. Xie, and S. Lin, "Local relation networks for image recognition," in *Proceedings of the IEEE/CVF International Conference on Computer Vision*, pp. 3464–3473, 2019.

- [20] P. Ramachandran, N. Parmar, A. Vaswani, I. Bello, A. Levskaya, and J. Shlens, "Stand-alone self-attention in vision models," *Advances in Neural Information Processing Systems*, vol. 32, 2019.
- [21] H. Zhao, J. Jia, and V. Koltun, "Exploring self-attention for image recognition," in *Proceedings of the IEEE/CVF Conference on Computer Vision and Pattern Recognition*, pp. 10076–10085, 2020.
- [22] X. Wang, R. Girshick, A. Gupta, and K. He, "Non-local neural networks," in *Proceedings of the IEEE Conference on Computer Vision and Pattern Recognition (CVPR)*, June 2018.
- [23] Z. Liu, Y. Lin, Y. Cao, H. Hu, Y. Wei, Z. Zhang, S. Lin, and B. Guo, "Swin transformer: Hierarchical vision transformer using shifted windows," in *IEEE International Conference on Computer Vision (ICCV)*, 2021.
- [24] W. Wang, E. Xie, X. Li, D.-P. Fan, K. Song, D. Liang, T. Lu, P. Luo, and L. Shao, "Pyramid vision transformer: A versatile backbone for dense prediction without convolutions," in *Proceedings of the IEEE/CVF International Conference on Computer Vision (ICCV)*, pp. 568–578, October 2021.
- [25] X. Chu, Z. Tian, Y. Wang, B. Zhang, H. Ren, X. Wei, H. Xia, and C. Shen, "Twins: Revisiting the design of spatial attention in vision transformers," *Advances in Neural Information Processing Systems*, vol. 34, 2021.
- [26] L. Yuan, Y. Chen, T. Wang, W. Yu, Y. Shi, Z. Jiang, F. E. Tay, J. Feng, and S. Yan, "Tokens-to-token vit: Training vision transformers from scratch on imagenet," 2021.
- [27] R. Child, S. Gray, A. Radford, and I. Sutskever, "Generating long sequences with sparse transformers," *arXiv preprint arXiv:1904.10509*, 2019.
- [28] I. Beltagy, M. E. Peters, and A. Cohan, "Longformer: The long-document transformer," *arXiv preprint arXiv:2004.05150*, 2020.
- [29] N. Kitaev, L. Kaiser, and A. Levskaya, "Reformer: The efficient transformer," *arXiv preprint arXiv:2001.04451*, 2020.
- [30] G. Daras, N. Kitaev, A. Odena, and A. G. Dimakis, "Smyrf-efficient attention using asymmetric clustering," *Advances in Neural Information Processing Systems*, vol. 33, pp. 6476–6489, 2020.
- [31] S. Wang, B. Z. Li, M. Khabsa, H. Fang, and H. Ma, "Linformer: Self-attention with linear complexity," *arXiv preprint arXiv:2006.04768*, 2020.
- [32] J. Lu, J. Yao, J. Zhang, X. Zhu, H. Xu, W. Gao, C. Xu, T. Xiang, and L. Zhang, "Soft: Softmax-free transformer with linear complexity," *Advances in Neural Information Processing Systems*, vol. 34, 2021.
- [33] Z. Shen, M. Zhang, H. Zhao, S. Yi, and H. Li, "Efficient attention: Attention with linear complexities," in *Proceedings of the IEEE/CVF Winter Conference on Applications of Computer Vision*, pp. 3531–3539, 2021.
- [34] Y. Zhong, P. Ji, J. Wang, Y. Dai, and H. Li, "Unsupervised deep epipolar flow for stationary or dynamic scenes," in *CVPR*, 2019.
- [35] J. Wang, Y. Zhong, Y. Dai, S. Birchfield, K. Zhang, N. Smolyanskiy, and H. Li, "Deep two-view structure-from-motion revisited," in *Proceedings of the IEEE/CVF Conference on Computer Vision and Pattern Recognition (CVPR)*, pp. 8953–8962, June 2021.
- [36] X. Cheng, Y. Zhong, Y. Dai, P. Ji, and H. Li, "Noise-aware unsupervised deep lidar-stereo fusion," in *CVPR*, 2019.
- [37] Y. Zhong, H. Li, and Y. Dai, "Open-world stereo video matching with deep rnn," in *ECCV*, 2018.
- [38] W. Sun, J. Zhang, and N. Barnes, "Inferring the class conditional response map for weakly supervised semantic segmentation," in *Proceedings of the IEEE/CVF Winter Conference on Applications of Computer Vision*, pp. 2878–2887, 2022.
- [39] J. Deng, W. Dong, R. Socher, L.-J. Li, K. Li, and L. Fei-Fei, "Imagenet: A large-scale hierarchical image database," in *2009 IEEE conference on computer vision and pattern recognition*, pp. 248–255, Ieee, 2009.
- [40] Y. Zhong, Y. Dai, and H. Li, "3d geometry-aware semantic labeling of outdoor street scenes," in *2018 24th International Conference on Pattern Recognition (ICPR)*, pp. 2343–2349, IEEE, 2018.
- [41] X. Chu, B. Zhang, Z. Tian, X. Wei, and H. Xia, "Do we really need explicit position encodings for vision transformers?," *arXiv e-prints*, pp. arXiv–2102, 2021.
- [42] K. Clark, U. Khandelwal, O. Levy, and C. D. Manning, "What does bert look at? an analysis of bert's attention," *arXiv preprint arXiv:1906.04341*, 2019.
- [43] O. Kovaleva, A. Romanov, A. Rogers, and A. Rumshisky, "Revealing the dark secrets of bert," *arXiv preprint arXiv:1908.08593*, 2019.
- [44] H. Minkowski, *Geometrie der zahlen*, vol. 40. Teubner, 1910.
- [45] R. R. Selvaraju, M. Cogswell, A. Das, R. Vedantam, D. Parikh, and D. Batra, "Grad-cam: Visual explanations from deep networks via gradient-based localization," in *Proceedings of the IEEE international conference on computer vision*, pp. 618–626, 2017.
- [46] W. Wang, E. Xie, X. Li, D.-P. Fan, K. Song, D. Liang, T. Lu, P. Luo, and L. Shao, "Pvtv2: Improved baselines with pyramid vision transformer," 2022.
- [47] A. Krizhevsky, G. Hinton, *et al.*, "Learning multiple layers of features from tiny images," 2009.
- [48] B. Zhou, H. Zhao, X. Puig, S. Fidler, A. Barriuso, and A. Torralba, "Scene parsing through ade20k dataset," in *Proceedings of the IEEE conference on computer vision and pattern recognition*, pp. 633–641, 2017.
- [49] H. Touvron, M. Cord, M. Douze, F. Massa, A. Sablayrolles, and H. Jégou, "Training data-efficient image transformers distillation through attention," 2021.
- [50] J. Xu, Y. Pan, X. Pan, S. Hoi, Z. Yi, and Z. Xu, "Regnet: Self-regulated network for image classification," 2021.
- [51] A. Ali, H. Touvron, M. Caron, P. Bojanowski, M. Douze, A. Joulin, I. Laptev, N. Neverova, G. Synnaeve, J. Verbeek, *et al.*, "Xcit: Cross-covariance image transformers," *Advances in neural information processing systems*, vol. 34, 2021.
- [52] S. Xie, R. Girshick, P. Dollár, Z. Tu, and K. He, "Aggregated residual transformations for deep neural networks," 2017.
- [53] D. P. Kingma and J. Ba, "Adam: A method for stochastic optimization," 2017.
- [54] I. Loshchilov and F. Hutter, "Sgdr: Stochastic gradient descent with warm restarts," *arXiv preprint arXiv:1608.03983*, 2016.
- [55] I. Radosavovic, R. P. Kosaraju, R. Girshick, K. He, and P. Dollár, "Designing network design spaces," 2020.
- [56] A. Kirillov, R. Girshick, K. He, and P. Dollár, "Panoptic feature pyramid networks," in *Proceedings of the IEEE/CVF Conference on Computer Vision and Pattern Recognition*, pp. 6399–6408, 2019.
- [57] T. Xiao, Y. Liu, B. Zhou, Y. Jiang, and J. Sun, "Unified perceptual parsing for scene understanding," in *Proceedings of the European Conference on Computer Vision (ECCV)*, pp. 418–434, 2018.